

# Steady State Handling

Giorgio Zampieri, Joel Serrao, Gabriel Crivat

## Introduction

The model given consisted in a double track model with vehicle parameters and tire coefficients from a formula SAE car. The reference frame convention used is **ISO**.

To produce the wanted *Speed Ramp Test* and *Steer Ramp Test*, the Simulink input blocks were modified in order to achieve the correct speed and steer profiles as desired inputs.

The first test performed was the speed ramp test.

## Speed Ramp Test

The desired forward speed profile provided to the controller consisted of a linear ramp starting from 0 km/h, speed kept for the first second, and then growing with slope  $0.2 \text{ m/s}^2$  up to 70 km/h. Regarding the desired steering angle, it was increased linearly and then kept constant with a value of  $20^\circ$ .

From the output of the simulation is possible to observe the linear growth of forward speed (1) and a behaviour close to the desired steady state wanted (2).

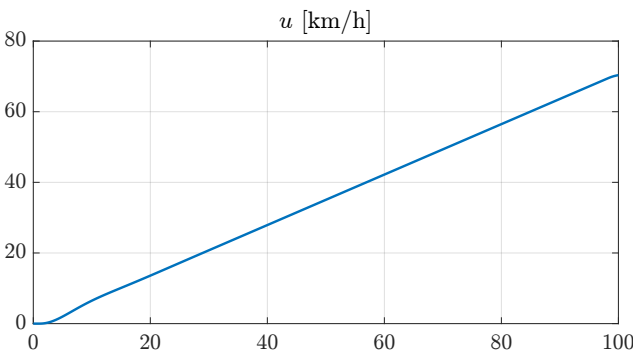


Figure 1: Vehicle Forward Speed

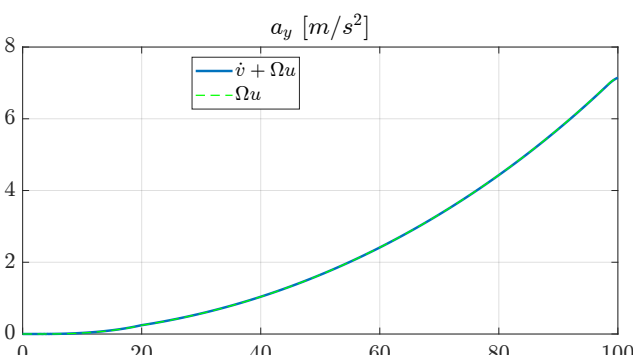


Figure 2: Steady State vs Dynamic Behaviour

Furthermore, the vehicle path shows a collapsing tra-

jectory, i.e. a decreasing radius, highlighting the **oversteering** behaviour of the car (3).

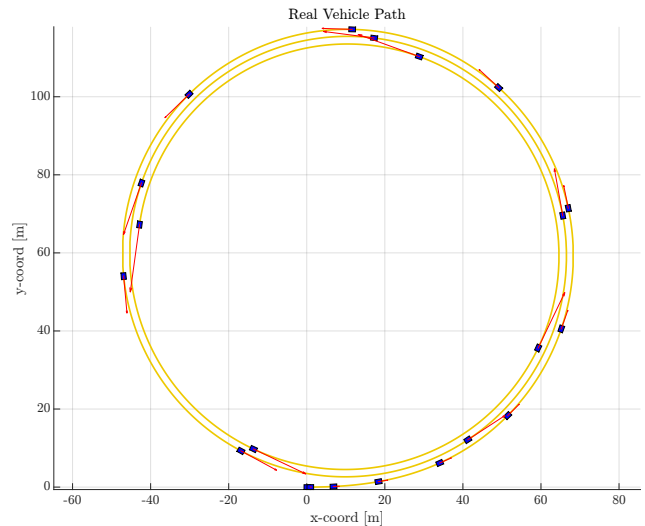


Figure 3: Vehicle Path

## Lateral Load Transfer

To estimate the lateral load transfer two approaches were used: the theoretical formula adding elastic and instantaneous contributions:

$$\begin{aligned}\Delta F_{zf} &= ma_y \left( \frac{L_r h_{rf}}{LW_f} + \frac{h_s}{W_f} \epsilon_\phi \right) \\ \Delta F_{zr} &= ma_y \left( \frac{L_f h_{rr}}{LW_r} + \frac{h_s}{W_r} (1 - \epsilon_\phi) \right)\end{aligned}\quad (1)$$

and the average of the normal loads on the tires from the simulation:

$$\begin{aligned}\Delta F_{zf} &= \frac{F_{z,fr} - F_{z,fl}}{2} \\ \Delta F_{zr} &= \frac{F_{z,rr} - F_{z,rl}}{2}\end{aligned}\quad (2)$$

Plotting them together in time (4) and the nominal ones in lateral acceleration (5):

For a positive turn we observe the lateral load transfer growing with lateral acceleration. The load transfer is bigger on the rear axle as expected, being stiffer than the front axle ( $K_{sf} = 1.67 \times 10^4 \text{ N/m}$ ,  $K_{sr} = 2.06 \times 10^4 \text{ N/m}$ ).

## Axle Characteristics

To compute the normalized axle characteristics, at first the axle apparent side slip were obtained averaging the

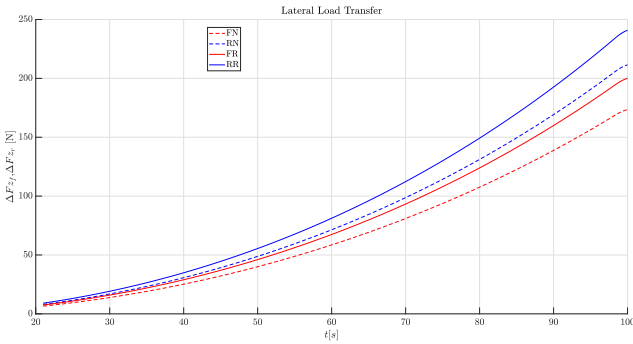
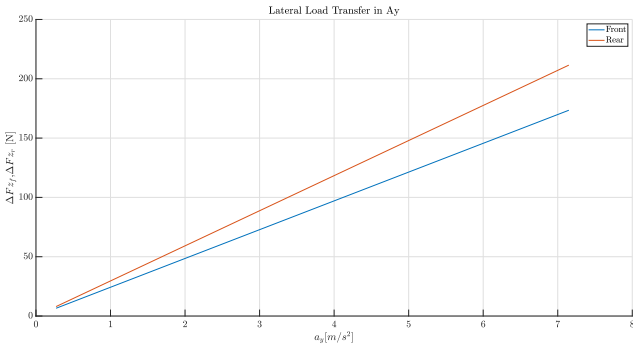


Figure 4: Lateral Load Transfer in time

Figure 5: Lateral Load Transfer in  $a_y$ 

tire side slips on each axle. These results were then compared with the ones obtained from the following formulae (**eq.3**) and verified they matched.

$$\begin{aligned} \alpha_f &= \delta_H \tau_H - \beta - \rho_0 L_f \\ \alpha_r &= -\beta + \rho_0 L_r \end{aligned} \quad (3)$$

The axle normal loads  $F_{zf}, F_{zr}$  were obtained by summing the tires normal loads, averaging out the lateral load transfer. The same method was applied to devise the axle lateral loads  $F_{yf}, F_{yr}$ . The axle characteristics could have been obtained also by using the following:

$$\begin{aligned} Y_f &= m a_y \frac{L_r}{L} \\ Y_r &= m a_y \frac{L_f}{L} \end{aligned} \quad (4)$$

Finally, the normalized axle characteristics, i.e. the axle adherence were obtained from **eq.5**:

$$\begin{aligned} \mu_f &= Y_f / F_{zf} \\ \mu_r &= Y_r / F_{zr} \end{aligned} \quad (5)$$

In figure (12) we can see the lateral loads on each tire for the axles, and the total lateral load. In figure (6) the normalized axle characteristics are showed.

By computing the gradient of the normalized axle characteristics the normalized cornering stiffness  $C_{yf}, C_{yr}$  are obtained.

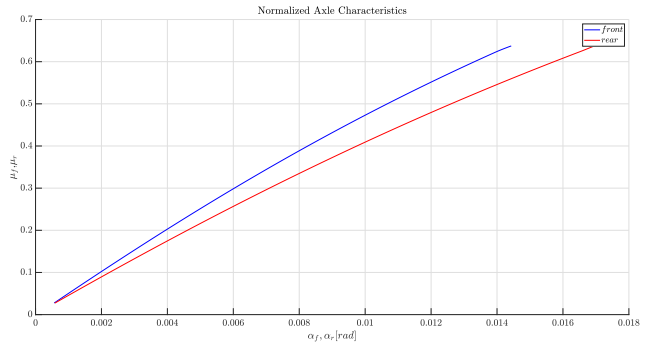


Figure 6: Normalized Axle Characteristics

## Handling Diagram

Starting from the steering behaviour of the vehicle:

$$\rho_0 L - \delta_H \tau_H = \alpha_r - \alpha_f \quad (6)$$

The difference  $-\Delta\alpha$  was plotted against normalized lateral acceleration. Using the function `polyfit` the linear part of the curve was fitted using a first order polynomial fit, hence, the only coefficient is the slope of the steering characteristics, i.e. the understeering gradient  $K_{US}$  which is negative with value of  $-3.42 \times 10^{-3}$ . Hence, the vehicle shows oversteering behaviour. This fitted value is smaller in modulus w.r.t. the theoretical understeering gradient  $-2.91 \times 10^{-3}$ , this is due to the settling time needed to reach the steady-state conditions, and the identification of the linear zone.

In the lower tiles of (13) the curvature and radius w.r.t. the normalized acceleration of the vehicle are showed, compared with the neutral behaviour. The radius is decreasing for higher lateral accelerations, highlighting an oversteering tendency, matching what was shown in the vehicle position graph.

## Yaw Rate Gain

The yaw rate gain  $\frac{\Omega}{\delta} = \frac{\rho u}{\delta} = \frac{u}{L(1+K_{US} u^2)}$  is shown in figure (7). The oversteering behaviour of the vehicle is clearly visible: being the steering angle kept constant, the growing curve represents an increase in yaw rate  $\Omega$  in speed due to growing curvature  $\rho$ , i.e. negative understeering gradient.

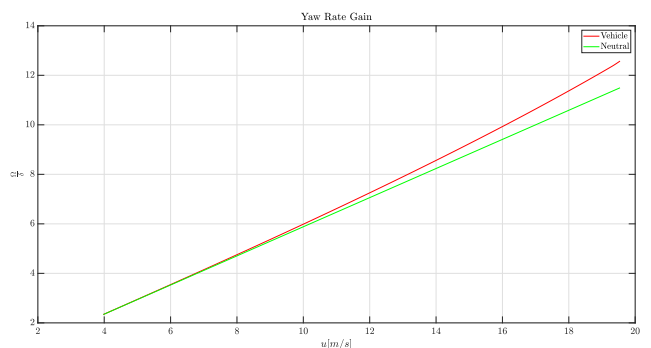


Figure 7: Yaw Rate Gain

## Body Slip Gain

The body slip gain  $\beta/\delta$  is shown in figure (8). To get the neutral curve a simple algebraic simplification was made, imposing  $\Delta\alpha = 0$ .

$$\begin{aligned}
 \frac{\beta}{\delta} &= \frac{L_r}{L} - \frac{\alpha_r L_f + \alpha_f L_r}{L\delta} \\
 &= \frac{L_r}{L} - \frac{(\Delta\alpha + \alpha_f)L_f + \alpha_f L_r}{L\delta} \\
 &= \frac{L_r}{L} - \frac{\alpha_f(L_f + L_r)}{L\delta} \\
 &= \frac{L_r}{L} - \frac{\alpha_f}{\delta}
 \end{aligned} \tag{7}$$

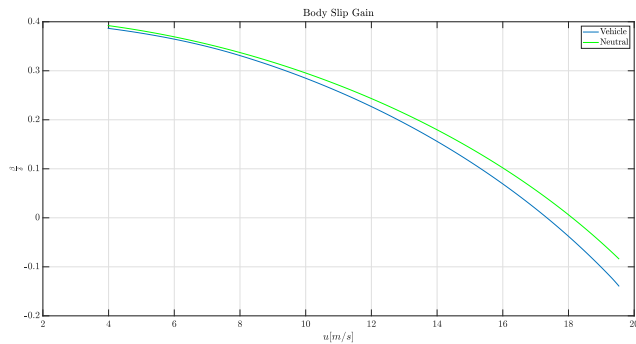


Figure 8: Body Slip Gain

## Effects of Parameters

In this final section the speed ramp test was performed varying camber angle, toe steer angle and rolling stiffnesses, in order to observe how the handling diagram would behave.

### Camber Effect

The camber angle of the tires was varied from  $-10^\circ$  and  $10^\circ$ , while keeping every other vehicle parameter constant. From (9) it is possible to observe that the handling characteristic changes its gradient, getting to a minimum value for negative camber angles. This happens due to camber force contribution to lateral force; when the camber is negative, i.e. the top part of wheel points inside, the camber force is reducing the lateral force necessary to balance the centrifugal force. The reduction of  $F_y$  means that the front axle presents a smaller side slip, thus  $\Delta\alpha = \alpha_r - \alpha_f$  grows, producing oversteering tendencies.

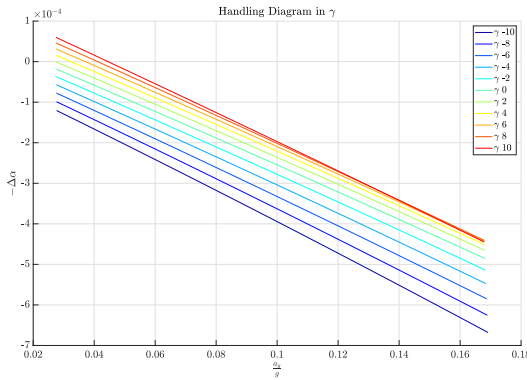


Figure 9: Camber Effect on Handling Diagram

### Toe Effect

The toe angle represents the wheel orientation in road plane; it has positive value when pointing inwards. The toe angle was added to the steering angle as a constant, paying attention to the sign ( $+\delta_0$  on the right and  $-\delta_0$  on the left). This parameter reduces the responsiveness of the steering, meaning that the car requires a larger steering input from the driver for the car to change direction. This makes the car more stable at high speeds and in long corners. The toe angle of the tires was varied from  $-1^\circ$  and  $1^\circ$ , while keeping every other vehicle parameter constant. From (10) it is possible to say that a toe angle different from zero causes an increase in the understeering behaviour, especially for negative toe angles (toe out). This is compatible with the reduced responsiveness.

### Roll Stiffness Effect

Varying the roll stiffness ratio between front to back the lateral load transfer varies. With respect to the handling diagram, from (11) the effects of  $\epsilon_\phi$  are observed. For values close to 0.1, i.e. a stiffer rear axle,

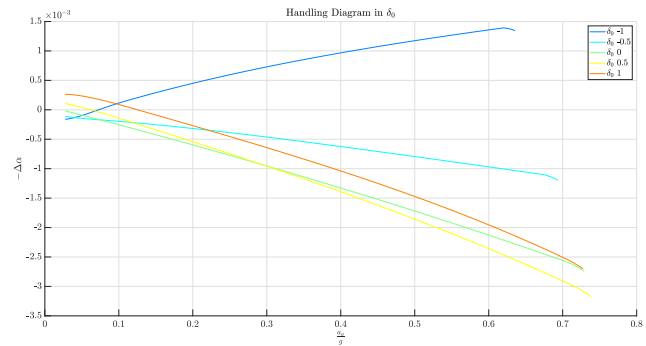


Figure 10: Toe Effect on Handling Diagram

the lateral load transfer grows on the rear. This unbalances the lateral forces, with the outer wheel lateral force entering in the non linear range while the inner stays in linear range, forcing the axle to increase its side slip to recover the force unbalance. This gives oversteering tendencies. The same holds when  $\epsilon_\phi \rightarrow 1$ , when the front axle is stiffer and slips more, causing understeering tendencies. Is worth knowing that the vehicle had a stiffness ratio of about  $\epsilon_\phi = 0.44$ , with behaviour showed in (13).

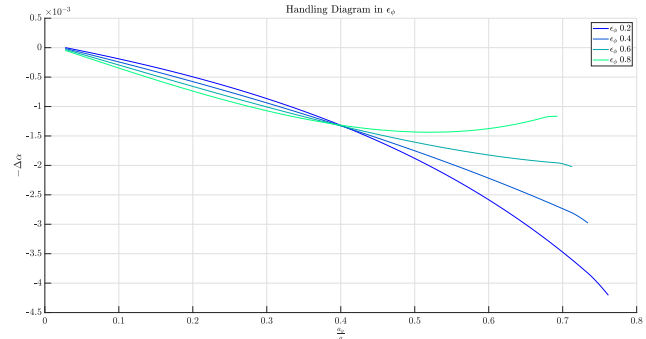


Figure 11: Roll Stiffness Effect on Handling Diagram

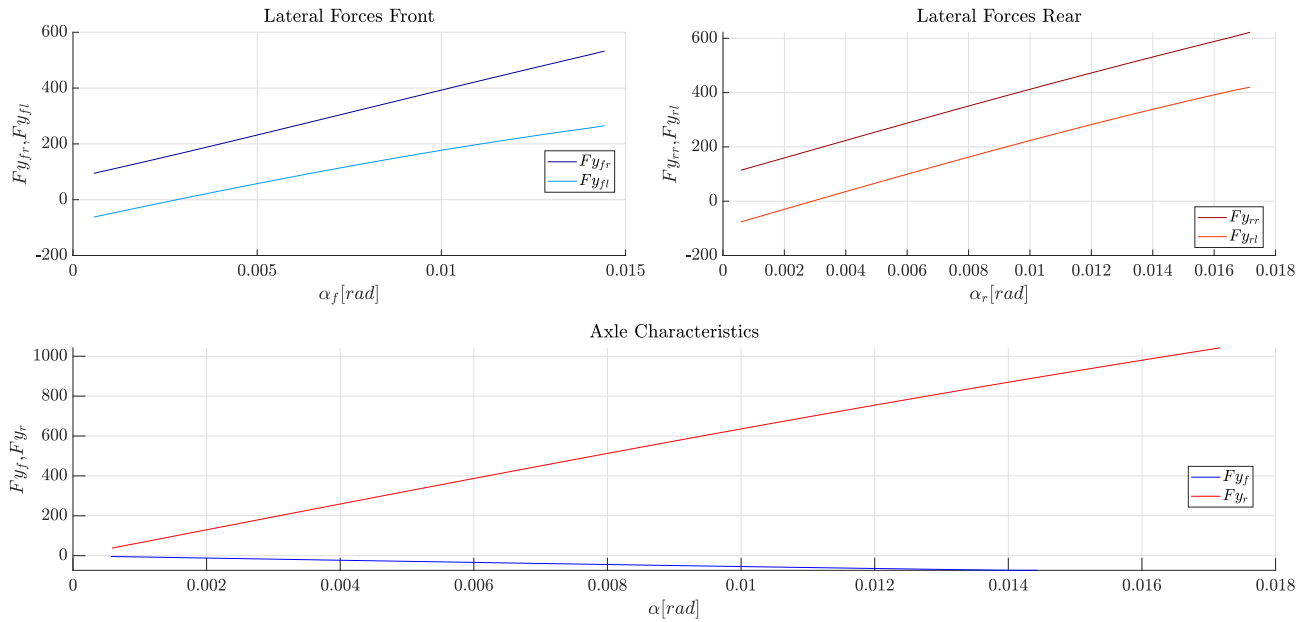


Figure 12: Axle Characteristics

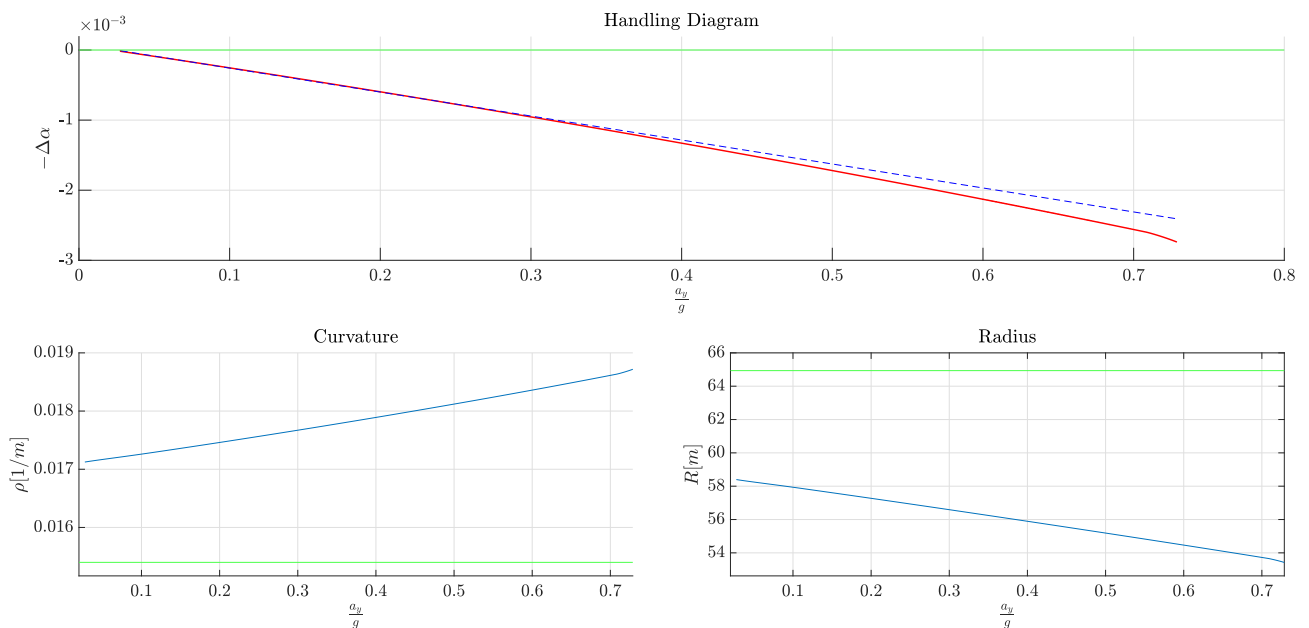


Figure 13: Steering Behaviour

## Steer Ramp Test

For the Steering Ramp test, the forward speed is initialized at 0 km/h, and the desired forward speed at the controller is set to 50 km/h. The steering angle is kept at 0° as long as the forward velocity does not stabilize, and then increased at a rate of  $0.25^\circ/\text{s}^2$ .

From the output of the simulation, it can be observed that the vehicle's forward speed is in transient conditions for the first twenty seconds before reaching steady-state conditions (14), with the lateral acceleration exhibiting behavior close to the desired steady-state (16).

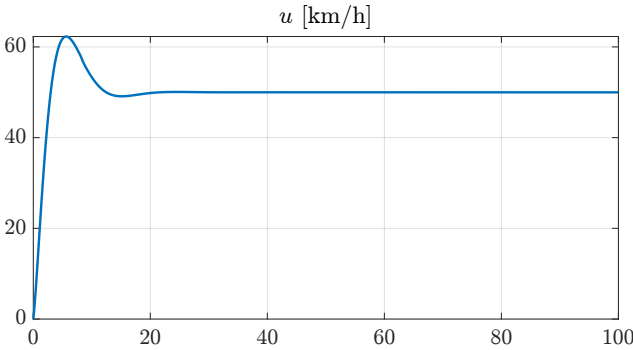


Figure 14: Vehicle Forward Speed

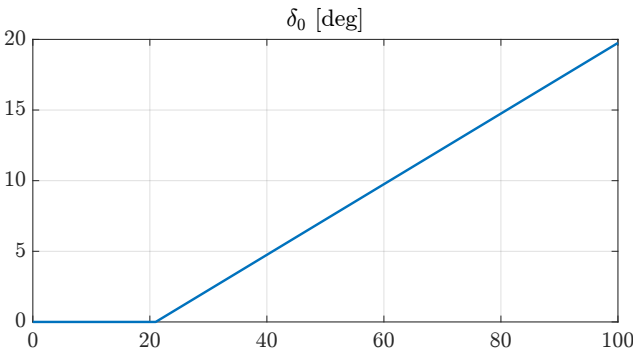


Figure 15: Steer Input

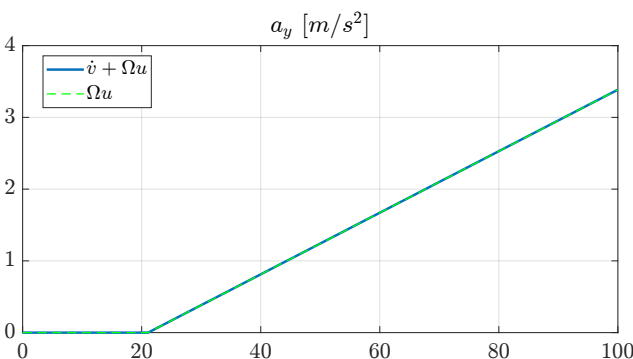


Figure 16: Steady State vs Dynamic Behaviour

Furthermore, in (17) the vehicle's trajectory can be observed.

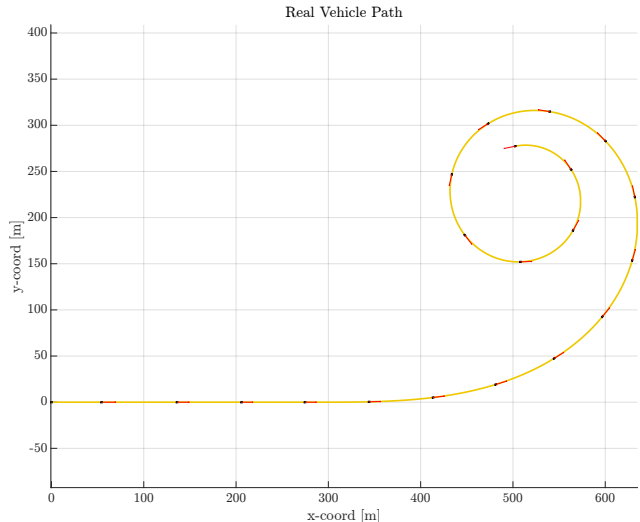


Figure 17: Vehicle Path

## Lateral Load Transfer

The theoretical formula, which includes both elastic and instantaneous contributions as shown in **eq.1**, is compared with the average of the normal loads on the tires obtained from the simulation (**eq.2**). Both curves are plotted together over time in **18**, and the nominal ones are plotted against lateral acceleration in **19**.

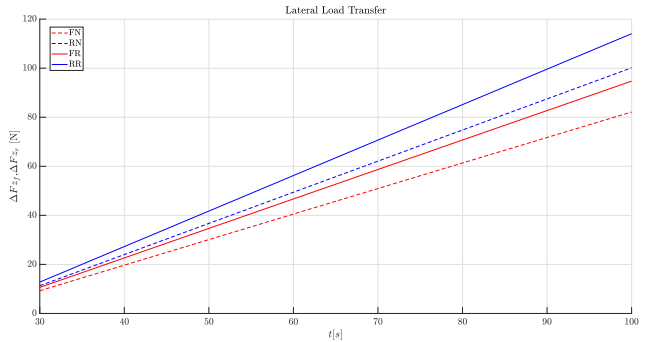


Figure 18: Lateral Load Transfer in time

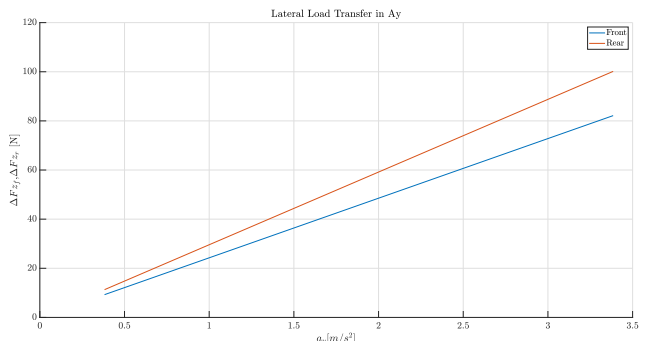


Figure 19: Lateral Load Transfer in  $a_y$

For a positive turn, it is observed that the lateral load transfer grows almost linearly with lateral acceleration. As expected, the load transfer is greater on the rear axle, which is stiffer than the front axle ( $Ks_f = 1.67 \times 10^4$  N/m,  $Ks_r = 2.06 \times 10^4$  N/m).

## Axle Characteristics

To compute the normalized axle characteristics, the axle apparent side slip was obtained by averaging the tire side slips on each axle. These results were then compared with the ones obtained from (eq.3) and verified that they matched.

The axle normal loads  $F_{z_f}$  and  $F_{z_r}$  were obtained by summing the tires normal loads and averaging out the lateral load transfer. The same method was applied to derive the axle lateral loads  $F_{y_f}$  and  $F_{y_r}$ .

Finally, the normalized axle characteristics, i.e. the axle adherence, were obtained from eq.5.

In figure (23), the lateral loads on each tire for the axles and the total lateral load are displayed. In Figure (20), the normalized axle characteristics are shown.

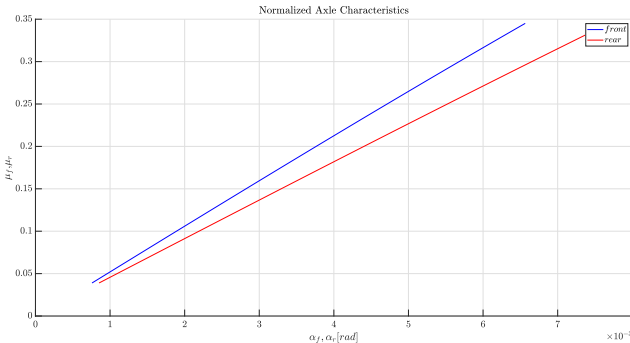


Figure 20: Normalized Axle Characteristics

By computing the gradient of the normalized axle characteristics, the normalized cornering stiffness  $C_{yf}$  and  $C_{yr}$  are obtained.

## Handling Diagram

The difference  $-\Delta\alpha$  was plotted against normalized lateral acceleration. Using the function `polyfit` the linear part of the curve was fitted using a first order polynomial fit, hence, the only coefficient is the slope of the steering characteristics, i.e. the understeering gradient  $K_{US}$  which is negative with value of  $-3.40 \times 10^{-3}$ . Hence, the vehicle shows oversteering behaviour. This fitted value is smaller in modulus w.r.t. the theoretical understeering gradient  $-2.48 \times 10^{-3}$ .

In the lower tiles of figure (23), the curvature and radius with respect to the normalized acceleration of the vehicle are displayed. As expected, the radius gradually decreases as the lateral acceleration increases.

## Effects of Parameters

In this final section, the steer ramp test was performed while varying the camber angle, and toe steer angle. The objective was to observe how the handling diagram would change under these different conditions.

### Camber Effect

The camber angle of the tires was varied from  $-8^\circ$  to  $8^\circ$ , while keeping every other vehicle parameter con-

stant. From (21), it is possible to observe that the handling characteristic changes its gradient, always maintaining its general oversteering behavior. However, it exhibits more oversteering for negative values of  $\gamma$ .

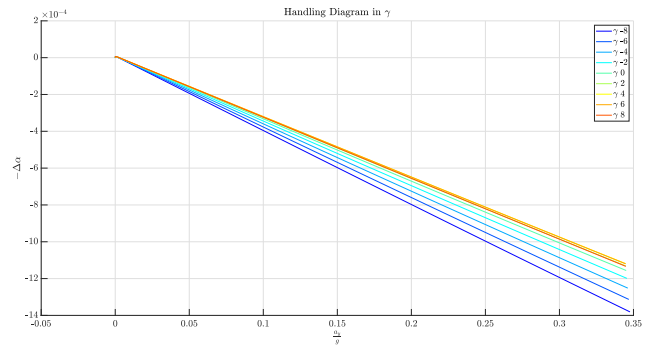


Figure 21: Camber Effect on Handling Diagram

### Toe Effect

The toe angle was varied from  $-1^\circ$  to  $1^\circ$  for the tires, while all other vehicle parameters were kept constant. From (22), it is evident that toe angle values different from zero lead to an increase in understeering behavior, especially for negative toe angles.

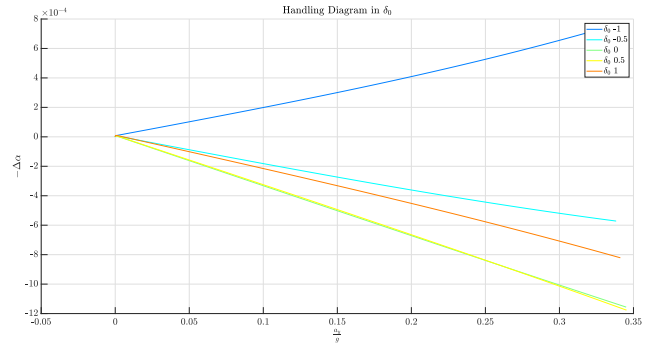


Figure 22: Toe Effect on Handling Diagram

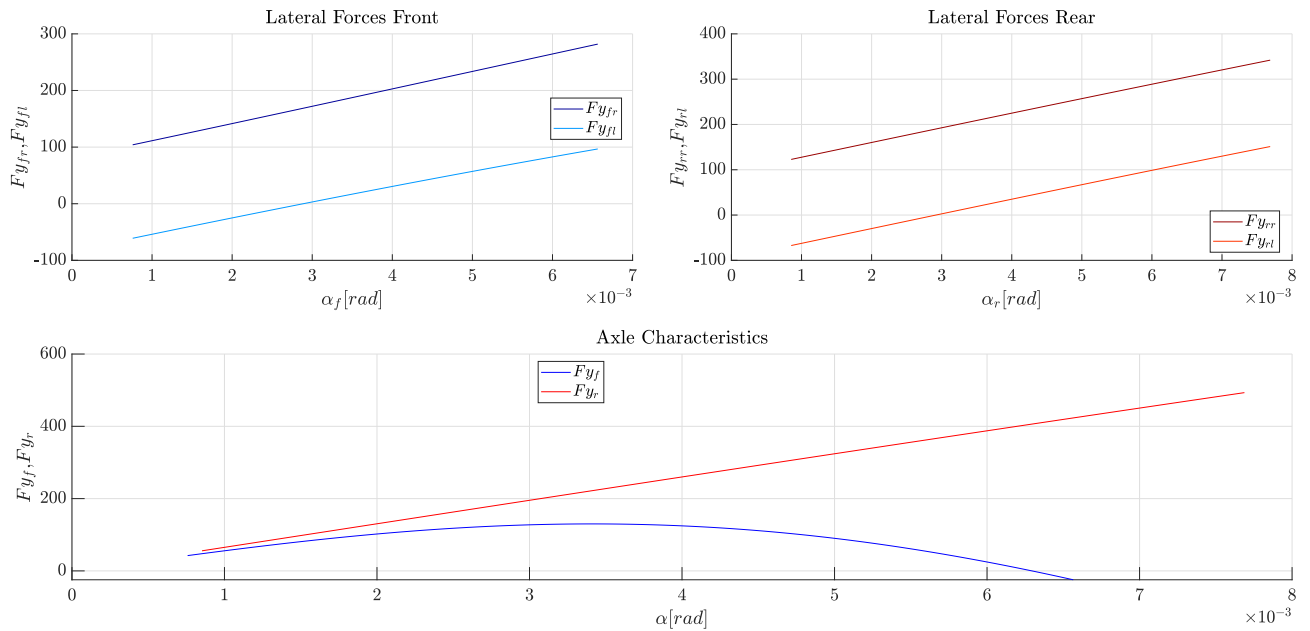


Figure 23: Axle Characteristics

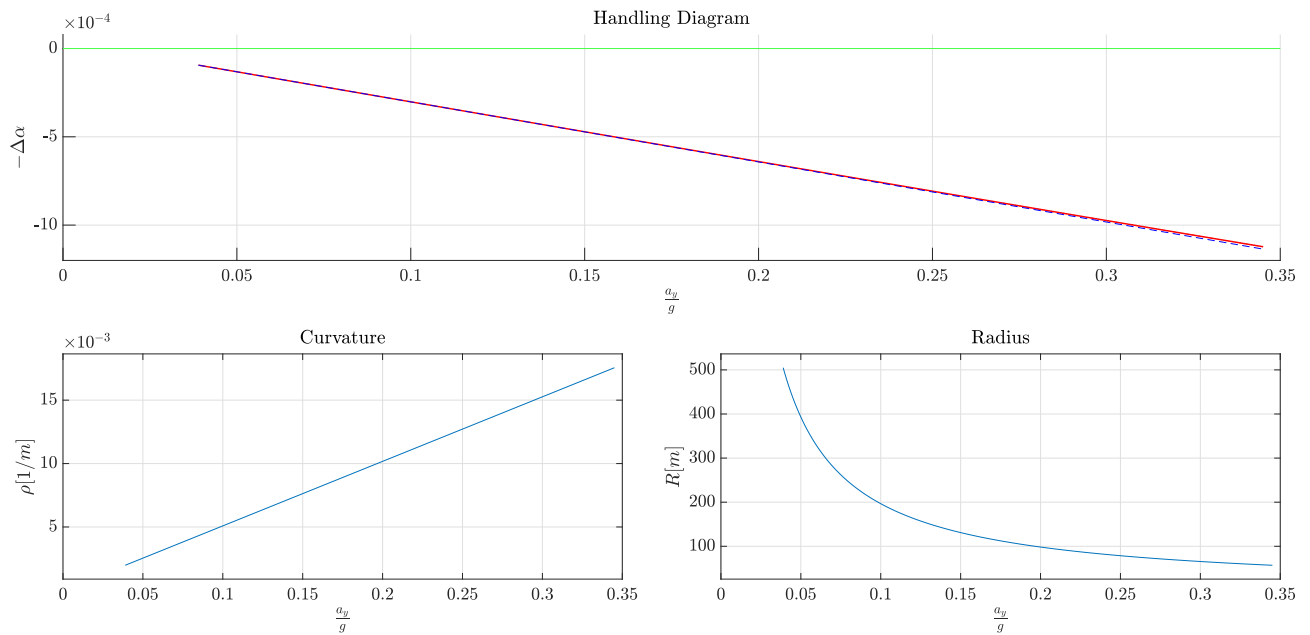


Figure 24: Steering Behaviour